International Journal of Bioprinting

RESEARCH ARTICLE

Performance of hybrid gelatin-PVA bioinks integrated with genipin through extrusion-based 3D bioprinting: An *in vitro* evaluation using human dermal fibroblasts

Syafira Masri[1], Manira Maarof[1], Izhar Abd Aziz[2], Ruszymah Idrus[1], Mh Busra Fauzi[1]*

[1]Centre for Tissue Engineering and Regenerative Medicine, Faculty of Medicine, Universiti Kebangsaan Malaysia, Cheras, Kuala Lumpur 56000, Malaysia

[2]3D Gens Sdn Bhd, 18, Jalan Kerawang U8/108, Bukit Jelutong, Shah Alam 40150, Malaysia

(This article belongs to the *Special Issue: 3D Printing in tissue engineering*)

Abstract

3D bioprinting technology is a well-established and promising advanced fabrication technique that utilizes potential biomaterials as bioinks to replace lost skin and promote new tissue regeneration. Cutaneous regenerative biomaterials are highly commended since they benefit patients with larger wound sizes and irregular wound shapes compared to the painstaking split-skin graft. This study aimed to fabricate biocompatible, biodegradable, and printable bioinks as a cutaneous substitute that leads to newly formed tissue post-transplantation. Briefly, gelatin (GE) and polyvinyl alcohol (PVA) bioinks were prepared in various concentrations (w/v); GE (6% GE: 0% PVA), GPVA3 (6% GE: 3% PVA), and GPVA5 (6% GE: 5% PVA), followed by 0.1% (w/v) genipin (GNP) crosslinking to achieve optimum printability. According to the results, GPVA5_GNP significantly presented at least 590.93 ± 164.7% of swelling ratio capacity and optimal water vapor transmission rate (WVTR), which is <1500 g/m^2/h to maintain the moisture of the wound microenvironment. Besides, GPVA5_GNP is also more durable than other hydrogels with the slowest biodegradation rate of 0.018 ± 0.08 mg/h. The increasing amount of PVA improved the rheological properties of the hydrogels, leading the GPVA5_GNP to have the highest viscosity, around 3.0 ± 0.06 Pa.s. It allows a better performance of bioinks printability via extrusion technique. Moreover, the cross-section of the microstructure hydrogels showed the average pore sizes >100 μm with excellent interconnected porosity. X-ray diffraction (XRD) analysis showed that the hydrogels maintain their amorphous properties and were well-distributed through energy dispersive X-ray after crosslinking. Furthermore, there had no substantial functional group changes, as observed by Fourier transform infrared spectroscopy, after the addition of crosslinker. In addition, GPVA hydrogels were biocompatible to the cells, effectively demonstrating >90% of cell viability. In conclusion, GPVA hydrogels crosslinked with GNP, as prospective bioinks, exhibited the superior properties necessary for wound healing treatment.

Keywords: 3D bioprinting; Wound healing; Tissue engineering; Bioinks; Gelatin; Polyvinyl alcohol; Genipin

***Corresponding author:**
Mh Busra Fauzi
(fauzibusra@ukm.edu.my)

Citation: Masri S, Maarof M, Aziz IA, *et al.*, 2023, Performance of hybrid gelatin-PVA bioinks integrated with genipin through extrusion-based 3D bioprinting: An *in vitro* evaluation using human dermal fibroblasts. *Int J Bioprint,* 9(3): 677.
https://doi.org/10.18063/ijb.677

Received: September 8, 2022

Accepted: December 2, 2022

Published Online: February 7, 2023

1. Introduction

The skin is the outermost layer of the human body. It significantly protects tissues from external harm by microorganisms while maintaining body dehydration and preventing electrolyte loss[1,2]. The skin is the most susceptible organ in direct contact with the external environment[3]. Certain groups of people may be exposed to highly risky infections or hazards, with severe consequences in common individuals, patients, and servants working in the healthcare sector[4]. A skin wound occurs due to the deterioration of the skin's normal anatomical structure and function[5]. According to the healing timeline, the wounds are classified as acute or chronic[6,7]. Surgical incisions and lacerations are common causes of acute wounds as well as abrasions. However, chronic wounds usually necessitate long-term care, and place a significant financial burden on the patients[8]. By 2027, the advanced wound care market is anticipated to reach a value of $18.7 billion, expanding at a compound annual growth rate of 6.6% from 2020 to 2027[9]. Optimal wound healing in adults should comprise four overlapping, continuous phases: inflammation, proliferation, remodeling, and hemostasis. However, chronic wounds with aberrant pathological characteristics result in a slow healing rate, prolonged inflammatory phase, and extensive scar development following recovery[10]. An ideal wound treatment should have better reproducibility, biocompatibility, cell adherence, and acceptable mechanical qualities.

An autologous split-thickness skin graft remains the gold-standard treatment for wounds of larger sizes. However, it has significant drawbacks due to donor site morbidity and the scarcity of donor tissue. Besides, allogeneic transplants carry significant risks due to graft versus host disease and persistent immunosuppression[11]. Previously, skin replacements failed due to contamination and flaws, with additional drawbacks of autologous and allografts treatments. Moreover, a clinical trial used an allogenic treatment with skin fibroblasts, keratinocytes, and polyglycolic/polylactic acids (DermaGraft™) that supply growth factors and extracellular matrix (ECM) to wounds with no immune rejection[12]. However, the instability of the ECM structure makes it susceptible to cellulitis and infections. Thus, tissue substitutes may be a potential strategy categorized under acellular and cellular skin substitutes[13]. Skin tissue engineering entails the creation of bioscaffolds resembling the microstructure of the native ECM. The bioscaffold provides a substrate for the cells to develop into solid tissue form, with biomolecules that serve as enhancers or supplements[14]. They have sufficient aquatic mobility and exceptional adhesion to host locations[15].

Three-dimensional (3D) bioscaffolds can be developed using conventional and advanced 3D bioprinting technologies[16]. It uses an additive manufacturing-based approach to create intricate 3D structures by depositing living cells, biomaterials, and other elements to form a 3D bioscaffold. Different bioprinting techniques are available, including extrusion-based bioprinting, inkjet bioprinting, laser-assisted bioprinting, and microfluidic-based bioprinting. However, extrusion-based bioprinting is the most widely used bioprinting technology with the excellent advantage of enabling rapid deposition of bioinks[17]. It offers excellent flexibility and reproducibility by fabricating 3D structures with a layer-by-layer deposition of bioinks through a virtual design through computer-aided design software[18,19]. Moreover, extrusion-based bioprinting also allows the deposition of high-viscosity bioinks, but typically it has lower printing precision.

Natural polymers, such as collagen, gelatin, and fibrinogen are commonly used as bioinks due to their excellent biodegradability and printability[20]. Gelatin, a collagen hydrolysis product, displays notable benefits for tissue engineering applications, including high biocompatibility, biodegradability, and the capability of preserving natural cell adhesion patterns. Depending on the source of the collagen and the hydrolytic treatment technique, there are several varieties of gelatin, such as Type A (porcine) and Type B (bovine), with various compositions[21]. In addition, gelatin is widely used in pharmaceutic and biomedical areas due to its low antigenicity and low *in vivo* inflammatory response[22]. The behavior of the gelatin solution depends on several factors, such as temperature, pH, concentration, and preparation method. A typical property of the gelatin solution is its capability to be gelled at low temperatures (about 20 – 30°C) by cooling to form hydrogels. The use of thermoresponsive gelatin-based hydrogels in extrusion-based 3D bioprinting has improved the ability to create solid 3D microstructures with a wide range of material as well as with a wide array of biological, chemical, physiological, and therapeutic functions[21]. It can be printed as a solid construct for cell survival accommodations or as sacrificial (or fugitive) "bioinks" for channel or pore designs. Several factors influence the gelatin-based hydrogels that are created and deposited during 3D printing procedures, including mechanical properties and stability of the hydrogels for *in vitro* and *in vivo* testing. However, gelatin has several drawbacks, such as low mechanical properties, rapid degradation rate, and limited thermostability, which restrict its future applications for wound treatment.

Polyvinyl alcohol (PVA) is a synthetic polymer that dissolves in water and is frequently used for 3D

bioprinting. Besides having excellent capability to improve mechanical strength, high swelling ratio, as well as the attributes of being biocompatible and non-toxic, PVA also has the benefit of post-polymerization modification because of its secondary hydroxyl groups. On the other hand, PVA has limitations in cell-biomaterial interactions and should be supplemented with other tissue-inducing materials to speed up the healing process[23]. Other research has shown that PVA has low protein affinities, which restrict cell binding or attachment and potentially lead to a rounded morphology. Therefore, this study incorporated PVA with gelatin to provide a conducive environment for cells to survive due to an arginine-glycine-aspartic acid integrin-binding sequence in the gelatin that involves both the A-chain and the B-chain[24].

The crosslinking process is one of the sustainable and well-known approaches to ensuring excellent stability of fabricated bioscaffolds before implantation. It can be divided into irradiation-, physical- and chemical-based methods. Genipin derived from the *Gardenia jasminoides* plant was used in fabricating gelatin-PVA hydrogels as a crosslinking agent. It was utilized as a crosslinking agent due to its potential to increase mechanical strength, stability and non-toxicity[25]. Briefly, the genipin combines with primary amine groups to fix biological tissues, and it is substantially less harmful than other chemical crosslinkers, such as glutaraldehyde, diisocyanates, and epoxides[26]. This study aims to develop a simple, accessible, and reproducible bioinks formulation for wound healing applications, and to evaluate the influence of genipin as a chemical crosslinker against gelatin-PVA bioinks. Besides, the physicochemical and rheological properties of the bioinks were evaluated after fabricated via 3D bioprinting approach. Finally, by varying the amount of PVA, this study aims to identify a composite bioscaffold with acceptable performance and biocompatibility for skin tissue engineering through *in vitro* testing.

2. Materials and methods

The study design was approved by the Universiti Kebangsaan Malaysia Research Ethics Committee (Code no. FF-2021-376 and JEP-2021-605). The research was performed in certified facilities under ISO 9001:2015 quality management system.

2.1. Preparation of gelatin-PVA hydrogels

0.3 g and 0.5 g of PVA powder (MERCK KGaA, Germany; partially hydrolyzed [≥85%], MW 70,000 g/mol) were dissolved in 10 mL of distilled water (dH_2O) for 1 h at 60°C to obtain 3% and 5% (w/v) concentration. 6 g of gelatin (GE) powder from (Nitta-Gelatin Ltd., Osaka, Japan) was weighed and added to the dissolved PVA mixture after the temperature cooled down at 40°C and stirred for 30 min until fully dissolved. Next, 0.1% of genipin (GNP) (FUJIFILM Wako Pure Chemical Corporation, Japan) was prepared by dissolving 0.01 g (w/v) of GNP powder in 70% of ethanol (EtOH; MERCK, Darmstadt, Germany). After the mixture became homogenous, the GNP was added into the GPVA mixture to obtain a final formulation of GE_GNP (0.1% GNP), GPVA3_GNP (3% PVA _0.1% GNP), and GPVA5_GNP (5% PVA_0.1% GNP) while the non-crosslinked hydrogels were represented as GE_NC, GPVA3_NC (3% PVA), and GPVA5_NC (5% PVA).

2.2. Synthesis of gelatin-PVA composite bioinks

Sterilized bioinks were prepared under the biosafety cabinet to maintain sterility using sterilized GE and PVA powder. Next, autoclaved distilled water (dH_2O) was used to dissolve the PVA powders at 60°C followed by dissolving the GE powder at 40°C. Sterilized GNP powder was dissolved in 70% ethanol before adding into the GPVA solution to obtain different hydrogels formulation GE_GNP, GPVA3_GNP, and GPVA5_GNP solution. Dissolved GPVA solutions were thoroughly mixed with human dermal fibroblasts (HDFs) with 1.5×10^6 of cell density per mL of gels for the subsequent 3D bioprinting process.

2.3. 3D bioprinting of gelatin-PVA hydrogel

A model was built by Autodesk fusion 360 software (stl. file format). The pre-defined structures were input into Simplify3D software (version 4.1). A 3D bioprinter, Biogens XI (3D Gens, Malaysia), was used to print GPVA bioinks. Sterilized GPVA bioinks were loaded into a sterilized printing syringe (inner diameter: 0.3 mm) at the tip, and the printing process was conducted using an extrusion-based printhead. The hydrogel was deposited via an extrusion-based bioprinting approach, and the material flow for the printhead was controlled by pressure regulators. The printability of different GPVA hydrogels was evaluated using a combination of different printing temperatures (27 – 19°C) and speed rates (4000 mm/s) using a constant nozzle diameter of 0.3 mm. The adjacent filaments were printed with 2.5 cm in length at 0.3 mm of retraction. Multi-layer layered hydrogel construct with grid-like patterns was fabricated by printing each layer of grid-like patterns directly over the previous layer using an optimal combination of speed rates and printing temperature. Figure 1 demonstrates the functional block diagram for 3D bioprinting process from the beginning until 3D model is constructed.

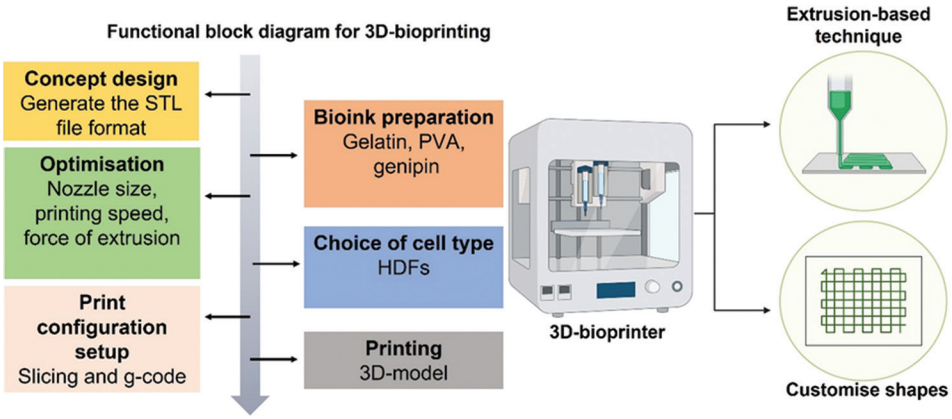

Figure 1. Functional block diagram for 3D bioprinting describing the preparation of 3D model using extrusion-based bioprinting technique. Image created with Biorender.com.

2.4. Evaluation of gross appearance

The gross appearance of the hydrogels, including a top and a cross-sectional view, was taken immediately after printing using a digital camera (Nikon, Tokyo, Japan). The post-printing width of 3D-printed hydrogels was compared to the width of the actual design using ImageJ software (V1.5, Bethesda, MD, USA).

2.5. Swelling ratio

The swelling behavior of the hydrogel was analyzed to evaluate its potential to absorb wound exudates for wound healing applications. The freeze-dried hydrogels were weighed to get the initial weight (W^1) before being submerged in phosphate-buffered saline (PBS; pH = 7.4) at room temperature until they achieved an equilibrium reading. The hydrogels were weighed to get the final weight (W^2) of the hydrogel. The swelling ratio percentage was determined using the following formula:

$$\text{Swelling ratio}(\%) = \frac{(W^2 - W^1)}{W^1} \times 100$$

2.6. Water vapor transmission rate (WVTR)

According to the American Society for Testing and Materials (ASTM) standard, the hydrogels were subjected to a WVTR test to measure their capacity to transmit water and enable gas exchange through the hydrogel to promote wound healing[27]. The hydrogel was positioned on top of the cylindrical cup filled with 10 mL of distilled water. The samples were then placed in an incubator with a controlled atmosphere of 5% CO_2 at 37°C. The results were recorded and analyzed using the formula below:

$$\text{WVTR} = \frac{(\text{W}^\text{i} - \text{W}^\text{f})}{(\text{A} \times \text{Time})}$$

Where W^i; initial weight, W^f; final weight, and A; for the bottle's surface area.

2.7. Enzymatic biodegradation

Enzymatic biodegradation testing was performed to assess the biodegradability of the hydrogels after they were introduced to the enzymatic reaction. The analysis was performed by weighing the initial weight (W^1) of the hydrogels before immersing the hydrogels into 0.0006% (w/v) collagenase type-I (Worthington, Lakewood, NJ, USA) in a 24-well plate and was incubated at 37°C for enzymatic reaction. The enzyme was then removed, and the hydrogels were washed using distilled water to remove the residual salts in the porous structure and were weighed to get the final weight (W^2) of the hydrogels. The weight loss percentage was calculated using the following equation:

$$\text{Weight loss}(\%) = \frac{(\text{W}^1 - \text{W}^2)}{\text{W}^1} \times 100$$

2.8. Contact angle

The printed hydrogels were used to determine the contact angle. A 10 µL of distilled water was dropped onto the surface of the hydrogel, and the images were captured using a digital camera. The contact angle was analyzed using ImageJ Software (National Institute of Health, V1.5, Bethesda, MA, USA).

2.9. Degree of crosslinking

The hydrogels' crosslinking degree was determined using the ninhydrin assay (Sigma Aldrich, Saint Louis, MO, USA). This analysis was performed to evaluate the free amino groups of the crosslinked hydrogels interacting with GNP compared with the NC hydrogels. The hydrogels were lyophilized for 24 h, and the hydrogels were weighed

at 10 mg for each scaffold. The samples were then boiled at 100°C for 2 min according to the protocol provided by the manufacturer. The amount of free amino groups was determined using a spectrophotometer (BioTek, PowerWave XS, Highland Park, IL, USA) and optical absorbance at 570 nm (Abs570). Besides, different concentrations of glycine (1.0, 0.5, 0.25, 0.125, and 0.625 mg/mL) were prepared as standard. The crosslinking degree was then calculated according to the following formula:

$$\text{Degree of crosslinking} = \frac{Amino^0 - Amino^1}{Amino^0} \times 100$$

Where $Amino^0$ is the absorbance of non-crosslink hydrogel, and $Amino^1$ is the absorbance of crosslinked hydrogel.

2.10. Antioxidant activity

The 2,2-diphenyl-1-picrylhydrazyl (DPPH) and 2,2'-azinobis-(3-ethylbenzthiazoline-6-sulfonate) ($ABTS^+$) assays (Sigma, >98% HPLC) were used to determine the antioxidant activity of hydrogel samples. Next, the hydrogels were then immersed in medium and kept at 37°C for 3 days to produce leachate media. In DPPH test, a fresh DPPH/ethanol (0.01 µm) solution was used for the measurements. 5 µL of leachate media were added in 195 µL of 100 µM DPPH solution and allow to stand at room temperature for 20 min. The absorbance change at 515 nm was measured using a spectrophotometer at 734 nm. The DPPH radical scavenging activity was calculated using the following formula:

$$\text{Scavenging activity}(\%) = \frac{Abc - Abs}{Abc} \times 100$$

Where *Abc* is the absorbance of control, and *Abs* is the absorbance of DPPH solution mixed with hydrogel samples. Each group had triplicate samples.

For the 2,2-azinobis-(3-ethylbenzothiazoline-6-sulfonate) $ABTS^+$ assay, potassium persulfate ($K_2S_2O_8$) (104 mM) was added to ABTS solution in water (1 mL, 7 mM) and reacted for 12 – 16 h in the dark to generate an $ABTS^+$ radical cation solution. The $ABTS^+$ solution was diluted to a certain concentration with absolute ethanol to obtain a working solution with an initial absorbance reading of 0.7 ± 0.2. Following that, 10 µL of samples and control were added to each well of the 96-well plate. After that, 90 µL of ABTS solution was added into each well and incubated for 4 min in the dark. The scavenging ability was calculated for each sample according to the absorbance of solvent at 734 nm, and the calculation was similar to what was done to estimate the antioxidant capacity by the DPPH assay.

2.11. Rheological characterization

The viscoelastic characteristics of the hydrogels were measured at 23°C using an AR2000 rheometer (TA Instruments) with a parallel plate geometry (20 mm) and a gap of 2000 µm. The storage modulus (G'), loss modulus (G"), and complex viscosity (η*) of the hydrogels were determined using an oscillating mode-frequency sweep at 23°C with an angular frequency in the range of 0.1 rad/s to 100 rad/s. The viscosity (η) of the bioinks under different temperatures was evaluated using a flow temperature-ramp with a start temperature of 27°C and an end temperature of 19°C.

2.12. Porosity degree

The hydrogels were lyophilized prior to the porosity assessment through a liquid displacement method that was adapted from Ghaffari *et al.* (2020) with some modifications[28]. Absolute ethanol (99.5% EtOH) was chosen as the displacement liquid due to its capability to penetrate the pores of the hydrogel without causing shrinkage or swelling of the matrix. The initial weight (*W*) and the volume (V) of the lyophilized hydrogels were recorded before being immersed in absolute ethanol for 24 h. The excess ethanol was then gradually wiped away using filter paper (Whatmann®, No.42, Merck, Darmstadt, Germany), and the weight of the hydrogel after immersion (*W"*) was recorded. The porosity was then calculated using the following equation:

$$\text{Porosity}(\%) = \left[\frac{(W'' - W)}{(\rho \times \text{V})}\right] \times 100$$

Where ρ is the density of the 99.5% EtOH.

2.13. Scanning electron microscopy (SEM)

Field emission scanning electron microscopy (FESEM; Supra 55VP model, Jena, Germany) was used to examine the cross-sectional microstructure of hydrogels. Before analysis, the lyophilized hydrogels were coated with an ultra-thin layer of gold by ion sputtering. ImageJ software (V1.5, Bethesda, MD, USA) was then used to randomly measure the average pore sizes of the hydrogel.

2.14. Atomic force microscopy (AFM)

The surface roughness of the lyophilized hydrogel was characterized using an atomic force microscope (AFM) analyzer (Park Systems, NX-10, Korea). The XEI Image Processing Program was used to analyze the AFM photographs, and the roughness of the scaffold surface was assessed. Surface roughness assessment was performed on a sample with a sample size 5 × 5 of mm using non-contact

mode scanning at 0.2 Hz (scan size 5 and 2 nm) and pixels of 256 × 256.

2.15. Chemical characterization

Fourier transform infrared (FTIR) spectra of hydrogel formulations were obtained using an FTIR spectrometer (PE, Waltham, MA, USA) to detect the crosslinked structure and intermolecular interactions between GPVA and GNP functional groups in the range of 4000 cm^{-1} to 500 cm^{-1} wavelengths. The absorbance peaks were discovered to determine the chemical structure and alterations after crosslinking. The determination of the crystalline and amorphous structures of the hydrogels were analyzed using an X-ray diffractometer (Bruker, D8 Advance, Coventry, UK) in the range of 0 – 80°C with a diffraction angle of (2θ). The diffractogram was further analyzed using the integrated software (Diffrac. Suite EVA, V4.0, Bruker, Coventry, UK). In addition, an energy dispersive X-ray (EDX) analysis was carried out to determine the existence of the element's composition in the hydrogels. A Phenom Pro X SEM EDX microscope (Phenom, Eindhoven, The Netherlands) was used to conduct this investigation. As a control, commercial gelatin, GNP, and PVA powder were employed.

2.16. Skin cell isolation and culture

Skin samples of six consented patients were taken as redundant tissue following the abdominoplasty procedures. Skin samples were sliced into tiny (1 – 2 cm) pieces and washed with sterilized Dulbecco's phosphate-buffered saline (DPBS). The skin was digested for 4 – 6 h in the shaker incubator with 0.6% collagenase Type I (Worthington-Biochemical Corporation), followed by trypsin-EDTA (Gibco, USA) 10 min. The cell suspension was centrifuged for 5 min at 5000 rpm before being resuspended with a co-culture medium containing Epilife (Gibco/BRL, Carlsbad, CA, USA) and F12: DMEM (Gibco/BRL, Carlsbad, CA, USA) in the same ratio (1:1) that was supplemented with 10% fetal bovine serum (FBS; Biowest, USA). The cells were then seeded in a 6-well culture plate at 1×10^4 cells/cm^2 and incubated at 37°C in 5% CO_2. The medium was changed for every 2 – 3 days. The cells were differentiated and trypsinized after achieving 70 – 80% confluency. The HDFs were expanded in a 75 cm^2 culture flask with F12:DMEM and 10% FBS.

2.17. Cytotoxicity test

The encapsulated cells in the hydrogels were tested for cell viability using a Live/Dead Cytotoxicity assay for mammalian cells (Thermo Fisher Scientific, Waltham, MA, USA) according to the manufacturer's recommendations. Sterilized bioinks were prepared by fabricating the sterilized GE, PVA, and GNP powder and were printed using a 3D bioprinter. The bioinks were encapsulated with HDFs with 1.5×10^6 per mL of cell density. Cell viability will be assessed 24 h after post-printing. After 30 min of treatment with 250 µL of a mixture of 2 mM acetoxymethoxy calcein derivate (calcein-AM) and 4 mM ethidium homodimer-1 (EthD-1) at 37°C, cell toxicity was assessed using a fluorescence microscope (Nikon A1R-A1, Japan) at ×100 magnification.

2.18. Proliferation of fibroblasts

3-(4,5-dimethylthiazol-2-yl)-2,5-diphenyl tetrazolium bromide (MTT) assay (Merck, Germany) was used to evaluate cellular survivability against crosslinked hydrogels GE_GNP, GPVA3_GNP, and GPVA5_GNP. The HDFs (1.5×10^6 of cell density), which were supplemented with DMEM:12 and 10% FBS (Gibco, USA), were encapsulated in the sterile bioinks and allowed to polymerize before incubation at 37°C with 5% CO_2. On days 1, 5, and 7, the culture media was removed, and 200 µL of pure medium containing 20 µL of 0.5 mg/mL MTT (Sigma-Aldrich, St. Louis, MO, USA) was added and incubated for 4 h at 37°C. Finally, the culture medium was replaced with 100 µL dimethyl sulfoxide (DMSO; Sigma-Aldrich, St. Louis, MO, USA) and put in a shaker incubator for 10 min at 37°C. In the last step, to quantify cell viability and proliferation, the optical absorbance of the supernatants was measured by ELISA microplate plate reader at 540 nm.

2.19. Cell morphology

The morphology of HDFs following interaction with the bioinks was observed using FESEM (Supra 55VP model, Jena, Germany). After printing the bioinks with HDFs at 1.5×10^6 per mL of cell density, the hydrogels were fixed with 4% paraformaldehyde overnight. The hydrogels were dehydrated based on protocol adapted from Busra *et al.* (2017) with some modifications by immersing them in a succession of ethanol solutions (30%, 50%, and 70% with 10 min each)[29]. The hydrogels were lyophilized using a freeze-dryer overnight before being sputter-coated with nanogold and SEM examination.

2.20. Scratch wound assays

The tip of a sterile pipette was used to scratch confluent HDFs monolayers in the center of each well. After removing the culture medium, the cells were washed with DPBS (Sigma-Aldrich) and grown in the biomaterial

leachate media. For each of the three biological samples ($n = 3$), three technical replicates were conducted. A Nikon A1R-A1 live-cell imaging microscopy was used to obtain pictures at 1-h intervals to estimate the wound-healing rate as follows:

$$\text{Healing progress}(\%) = \frac{\text{Initial area of the wound}\left(\mu m^2\right) - \text{Final area of the wound}\left(\mu m^2\right)}{\text{Initial area of the wound}\left(\mu m^2\right)} \times 100$$

2.21. Statistical analysis

All experiments were repeated at least 3 times ($n = 3$), and statistical analyses were performed at the significance level of $P < 0.05$ by one-way and two-way analysis of variance (ANOVA) using GraphPad Prism (V9.0, GraphPad Software Inc., San Diego, CA, USA).

3. Results

3.1. Gross appearance

Figure 2A indicates that the digital photograph of the 3D-bioprinted GPVA bioinks was printed with different layers (1 layer, 3 layers, and 5 layers) through extrusion-

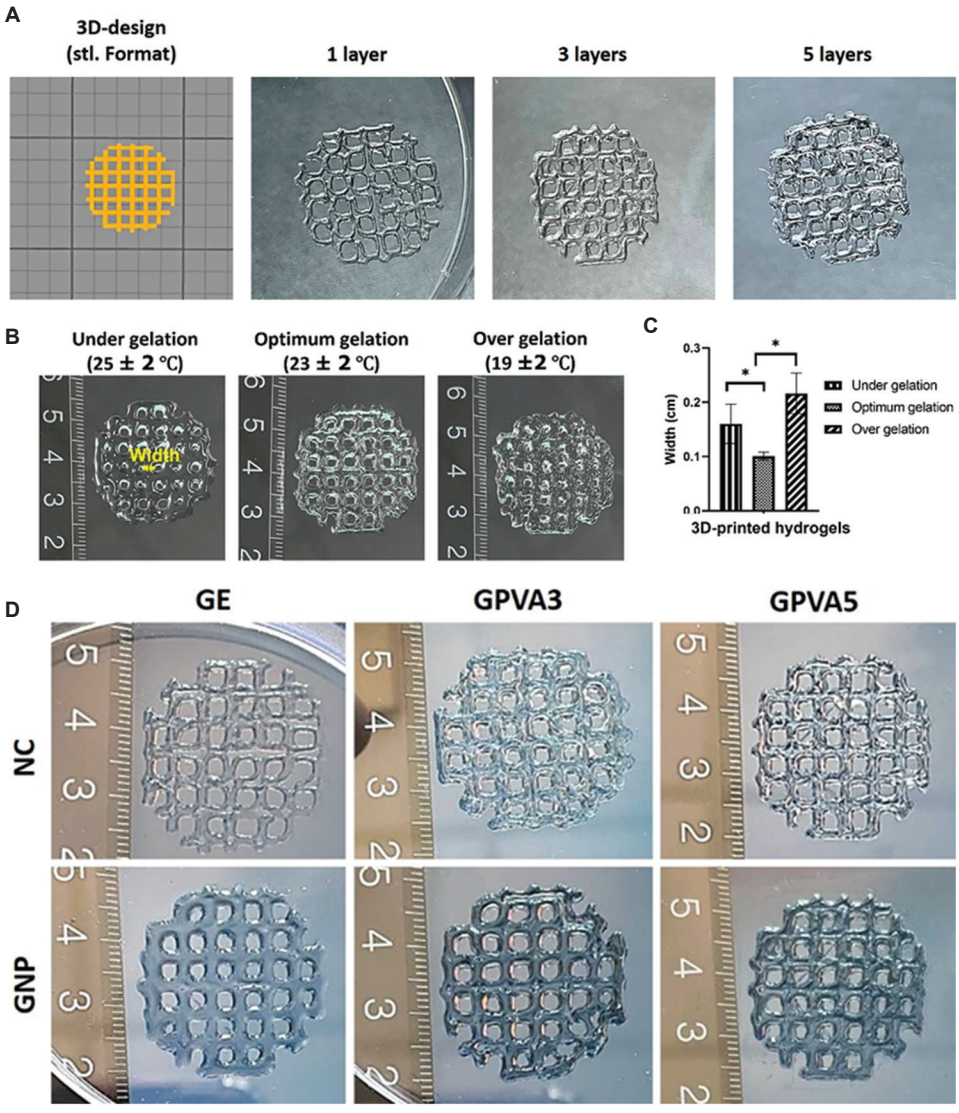

Figure 2. Gross appearance of the 3D-printed hydrogels. (A) Autocad design in stl. file followed by different layers of printed bioinks (1 layer, 3 layers, and 5 layers). (B) Optimization of printing temperature for the bioinks (under-gelation printed hydrogel (25 ± 2°C), optimum gelation printed hydrogel (23 ± 2°C), over-gelation printed hydrogel (19 ± 2°C). (C) Width evaluation of 3D-printed hydrogels. (D) Gross appearance of NC and GNP hydrogels for GE, GPVA3, and GPVA5.

based bioprinting. The top view images demonstrate that the hydrogels have a high printing precision to deposit bioinks up to 5 layers with better shape fidelity. Moreover, the printability assessment of the bioinks was evaluated against different printing temperatures (19 ± 2°C, 23 ± 2°C, and 25 ± 2°C) as shown in Figure 2B. The printed hydrogels' stability and shape fidelity decreased and slightly collapsed as temperature increased. However, the filaments printed at optimum temperature were thinner (0.1 ± 0.025 cm) than other filaments printed at under- and over-gelation (0.37 ± 0.03 and 0.21 ± 0.04 cm) as shown in Figure 2C. Next, six different types of bioinks formulations were printed using GE_NC, GPVA3_NC, GPVA5_NC, GE_GNP, GPVA3_GNP, and GPVA5_GNP through extrusion-based bioprinting, respectively. The hydrogels in Figure 2C were printed with 5 layers of bioinks and were characterized by well-defined individual printheads, as the composite hydrogels' grid is clearly seen at size 2.5 cm^2. Genipin (GNP) was used to construct and chemically crosslink gelatin-PVA hydrogels. Crosslinked hydrogels appeared bluish in color while non-crosslinked hydrogels appeared colorless after printing. Figure 2D shows the gross appearance of the 3D-bioprinted hydrogels for non-crosslink and crosslinked hydrogels.

3.2. Physical and antioxidant properties of 3D-bioprinted hydrogel

This study focused on fabricating GPVA hydrogels with crosslinked GNP through an extrusion-based bioprinting technique. The fabricated hydrogels were systematically characterized based on biodegradation rate, contact angle, swelling ratio, WVTR, degree of crosslinking, and antioxidant properties. The physicochemical analysis was evaluated for GNP and NC hydrogels, as shown in Figure 3. Hydrogels should possess multifunctional properties to accelerate wound healing. In wound healing applications, cellular skin replacements are designed with an appropriate biomaterial that can degrade while promoting a faster wound healing time frame. Adding GNP as a natural crosslinker and PVA helps improve the stability and control the biodegradability of the hydrogels, as stated in Figure 3A. The biodegradation rate of GPVA5_GNP was found to be the slowest (0.018 ± 0.08 mg/h) followed by GPVA3_GNP and GE_GNP (0.023 ± 0.21 mg/h and 0.062 ± 0.11 mg/h). However, all NC hydrogels were totally degraded within 1 h. The common factor of such assessment is hydrophilicity, which is related to the water contact angle and is reflected by the moisture content of the biomaterial[30]. The water contact angle values of the hydrogels are shown in Figure 3B. For GNP hydrogels, GE_GNP has the lowest contact angle (42.93 ± 3.2°), followed by GPVA3_GNP and GPVA5_GNP (49.36 ± 2.1° and 50.2 ± 1.2°). Besides, NC hydrogels GE_NC, GPVA3_NC, and GPVA5_NC have slightly larger contact angles compared to GNP hydrogels (44.8 ± 4.6°, 51.2±3.6°, and 53.5 ± 4.0°), respectively.

In wound healing applications, hydrogel was selected because its 3D networks are made up of hydrophilic polymers that expand in an aqueous solution and have the capacity to retain some water without dissolving. Figure 3C demonstrates that the swelling ratio of the

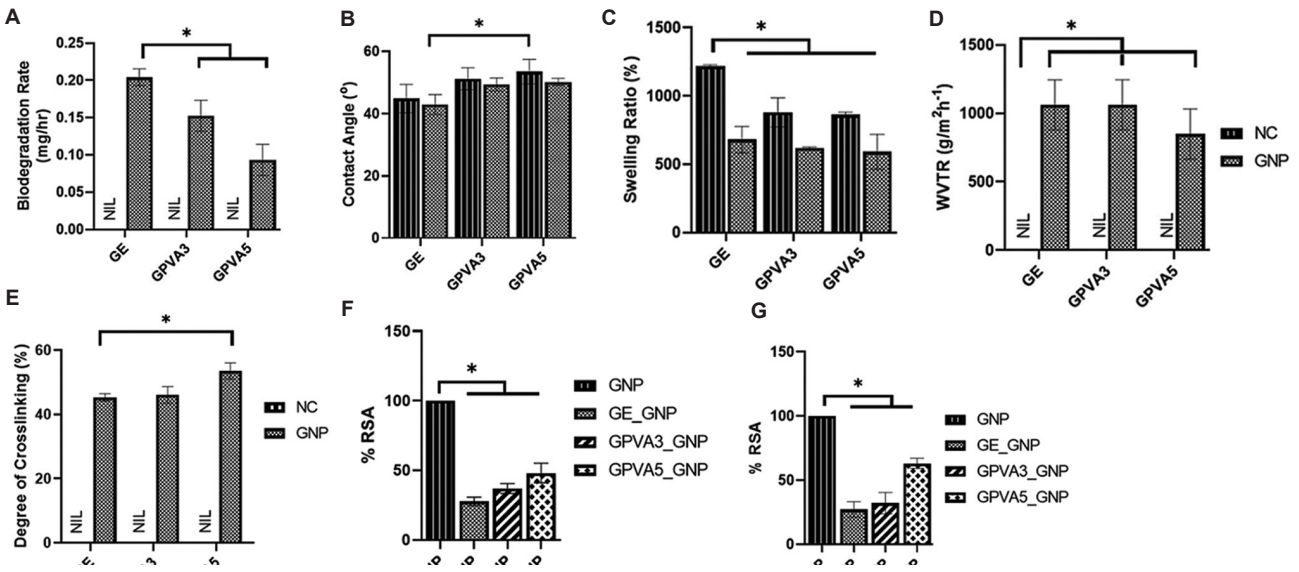

Figure 3. The physical and antioxidant analysis of 3D-printed hydrogels: (A) biodegradation rate, (B) contact angle, (C) swelling ratio, (D) water vapor transmission rate (WVTR), (E) degree of crosslinking, (F) DPPH assay, and (G) ABTS assay. *$P < 0.05$.

GE_GNP was 680.33 ± 177.4% and was significantly higher than the GPVA3_GNP and GPVA5_GNP (619.61 ± 218.4% and 590.93 ± 164.7%). The swelling ratio for GE_NC, GPVA3_NC, and GPVA5_NC was higher than those for GNP hydrogels (1217.11 ± 317.7%, 879.23 ± 57.4%, and 861.61 ± 114.2%). However, the swelling rate was slightly reduced in GPVA3_GNP and GPVA5_GNP hydrogels, which may be due to the strengthening of the pore structure of the hydrogel caused by GNP and PVA.

Next, the evaluation of the moisture level of the hydrogels was determined through WVTR in Figure 3D. To achieve optimal wound site conditions, the hydrogels should have an appropriate WVTR and an appropriate water absorption capacity to regulate fluid balance. GE_GNP has the highest WVTR (1096.90 ± 284.5 g/m²/h), followed by GPVA3_GNP and GPVA5_GNP (1026.24 ± 183.8 g/m²/h and 778.51 ± 183.8 g/m²/h, respectively). In Figure 3E, the GNP hydrogels had >40% average crosslinking degree. The results clearly demonstrate that hydrogels incorporated with higher concentrations of PVA, GPVA5_GNP (53.53 ± 2.54%) had a significantly higher level of crosslinking degree compared to GE_GNP only (46.57 ± 1.15%).

3.3. Antioxidant activity study

The hydrogel-incorporated with GNP demonstrated superior scavenging activity. GNP hydrogels had higher antioxidant activity than NC hydrogels. The DPPH assay result showed in Figure 3F shows that the addition of GNP to the GPVA hydrogels increased antioxidant capacity. The group of GPVA5_GNP showed superior free radical scavenging property according to the DPPH results, clearing over 45% of the free radicals, while the GPVA3_GNP and GE_GNP had a scavenging ratio of 37.0 ± 3.6% and 27.7 ± 3.1%, respectively. Moreover, ABTS scavenging activity also demonstrated the same trend as the DPPH assay as shown in Figure 3G.

3.4. Rheological properties of bioinks

Furthermore, the rheological analysis of hydrogels is demonstrated in Figure 4. The viscoelastic features of the hydrogels were investigated to correlate the intermolecular interaction forces with the hydrogel composition[31]. The hydrogels were tested for rheological properties for both NC and GNP hydrogels. The average viscosity in Figure 4A shows that the hydrogels have a similar trend in which viscosity increases from 27 Pa.s to 19 Pa.s. Moreover, as compared to the NC hydrogels, GPVA5_GNP, GPVA3_GNP, and GE_GNP have higher viscosity (3.0 ± 0.06 Pa.s, 0.2 ± 0.002 Pa.s, and 0.04 ± 0.01 Pa.s) compared to GPVA5_NC, GPVA3_NC, and GE_NC (0.7 ± 0.03 Pa.s, 0.06 ± 0.01 Pa.s, and 0.007 ± 0.009 Pa.s). This also proved that the addition of GNP and PVA promote higher viscosity to the hydrogels. Besides, based on the result in Figure 4B, the viscosity begins to drop at low frequency. The changes of complex viscosity (η*) arise from the different solvent varieties and solvent strengths. At 23°C, the complex viscosity of the crosslinked hydrogels began with GPVA5_GNP > GPVA3_GNP, and GE_GNP, (91384.2 ± 61415.71 Pa.s, 11259.0 ± 17946.09 Pa.s and 15947.3 ± 16810.76 Pa.s) at 0.1 rad/s as compared to the non-crosslinked hydrogels.

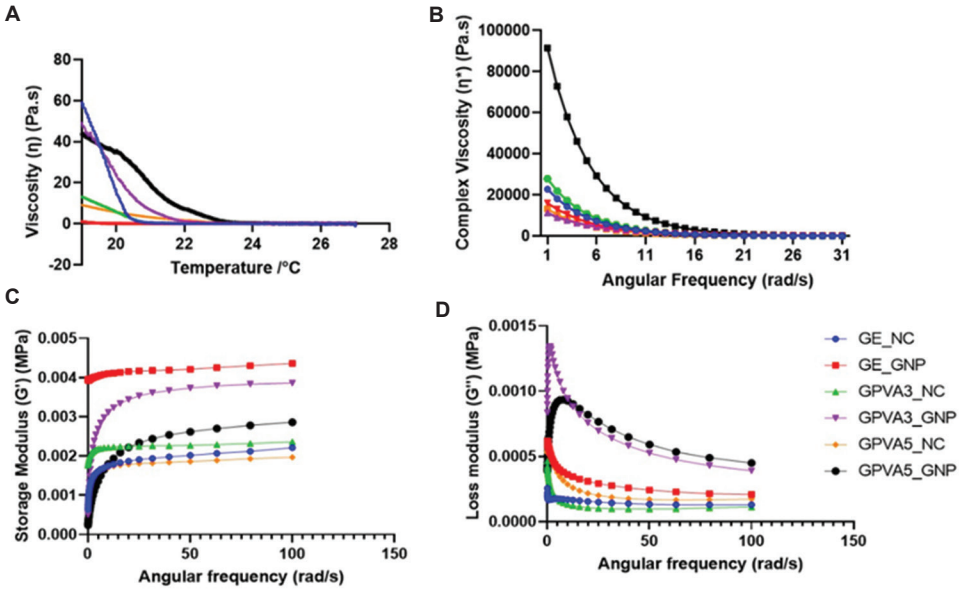

Figure 4. Rheological properties of the bioinks: (A) viscosity (η), (B) complex viscosity (η*), (C) storage modulus (G'), and (D) loss modulus (G"). *$P < 0.05$.

The frequency sweep curves of the hydrogels at 23°C are shown in Figure 4C and D. The hydrogels were demonstrated to have G' modulus greater than G" modulus over the entire frequency range, which is indicative of a gel-like nature. The value range for G' modulus was from 0.000234 ± 0.00083 mPa to 0.00396 ± 0.0037 mPa at a lower frequency (0.1 rad s^{-1}), for the following orders: GPVA5_GNP > GPVA3_GNP > GE_NC > GPVA5_NC > GPVA3_NC > GE_GNP, respectively. The GE_GNP showed the highest G' modulus value due to the absence of PVA in the hydrogel. This phenomenon occurred due to the PVA polymer that literally did not exhibit elastic behavior G'.

Compared to G', the decrease of G" confirms the advancement of stiffening and gel formation. The region where G' is less than G" suggests that viscosity is dominant, whereas the region where G' is more than G" reveals that elasticity is dominant due to an extension of hydrophobic interaction[32]. The value of G" was higher in GPVA5_GNP and GPVA3_GNP (0.0047 ± 0.000030 mPa and 0.00041 ± 0.000029 mPa, respectively) as compared to GE_GNP, GPVA5_NC, GPVA3_NC, and GE_NC.

3.5. Chemical characterization

The X-ray diffraction (XRD) patterns of NC and GNP hydrogels are shown in Figure 5A. Gelatin has a distinctive triple-helical crystalline structure, with two large peaks at 9.60° and 20°. The addition of PVA and Genipin (GNP) into gelatin hydrogels displayed a wide peak at 2θ=20°. Table 1 presents the amount of crystallinity and amorphous level of the hydrogels. According to the result, the presence of gelatin, PVA, and genipin inhibited the crystallization of crosslinked and non-crosslinked hydrogels.

The structural change of GPVA hydrogel before and after crosslinking was determined by FTIR analysis. The FTIR spectra of gelatin in Figure 5B show peaks at 3287.27 cm^{-1} (Amide A) and 2923.7 cm^{-1} (Amide B) due to -NH stretching of secondary amide, C=O stretching at 1631.23 cm^{-1} (Amide I), 1528.35 cm^{-1} (Amide II), and 1237.43 cm^{-1} (Amide III). The FTIR spectra of PVA show a broad peak around 3336.2 cm^{-1}, indicating stretching of hydroxyl groups and peaks at 2918.97 cm^{-1} and 1729.83 cm^{-1} due to C-H stretching. In NC hydrogels that were incorporated with PVA, the spectra reading showed the presence of peak at 3275.78 cm^{-1}, 3274.15 cm^{-1}, 3291.70 cm^{-1}, and 3292.1 cm^{-1} in GPVA3_NC, GPVA3_GNP, GPVA5_NC, and GPVA5_GNP, respectively, indicating the presence of hydroxyl group in the hydrogels. The presence of peaks below 1000 cm^{-1} was observed in crosslinked hydrogels, indicating the formation of intra- and inter-molecular crosslinking bonds by forming a heterocyclic structure of genipin with primary amine groups. Based on the peaks,

Table 1. The amount of crystallinity and amorphous level of the hydrogels

Hydrogels	Crystallinity (%)	Amorphous level (%)
GE_NC	25.5	74.5
GE_GNP	29.3	70.7
GPVA3_NC	24.0	76.0
GPVA3_GNP	25.3	74.7
GPVA5_NC	17.4	82.6
GPVA5_GNP	19.8	80.2

Table 2. Elemental composition of carbon (C), oxygen (O), and nitrogen (N) using energy dispersive x-ray

Hydrogels	C (%)	O (%)	N (%)
GE_NC	51.40±2.9	22.8±2.4	25.84±3.6
GE_GNP	47.83±2.9	24.80±2.1	27.40±3.5
GPVA3_NC	60.28±2.05	25.20±1.65	14.52±2.40
GPVA3_GNP	62.52±0.72	23.0±0.40	14.50±0.85
GPVA5_NC	61.60±3.12	23.98±2.04	10.02±3.54
GPVA5_GNP	58.58±3.74	25.88±2.71	15.60±4.34

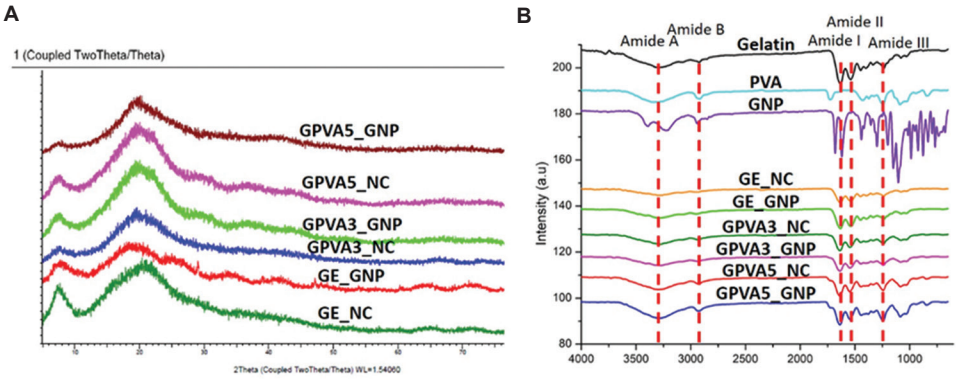

Figure 5. Chemical characterization of the 3D-printed hydrogels. (A) X-ray diffraction analysis. (B) Fourier transform infrared analysis.

there were no significant changes in the crosslinked hydrogels compared to the non-crosslinked hydrogels, indicating that the incorporation of GNP and PVA does not alter the native amorphous property of the hydrogels.

The elemental composition of the hydrogels for carbon (C), oxygen (O), and nitrogen (N) was evaluated through EDX as stated in Table 2. The EDX signals demonstrate that addition of PVA to the gelatin hydrogels impacted the rise in the proportion of C components in the scaffolds. The crosslinked hydrogels caused a minor decrease in carbon and a rise in oxygen components, but no significant change was detected.

3.6. 3D microstructure analysis

SEM images were obtained to aid in visualizing pore morphology and measuring pore diameters in

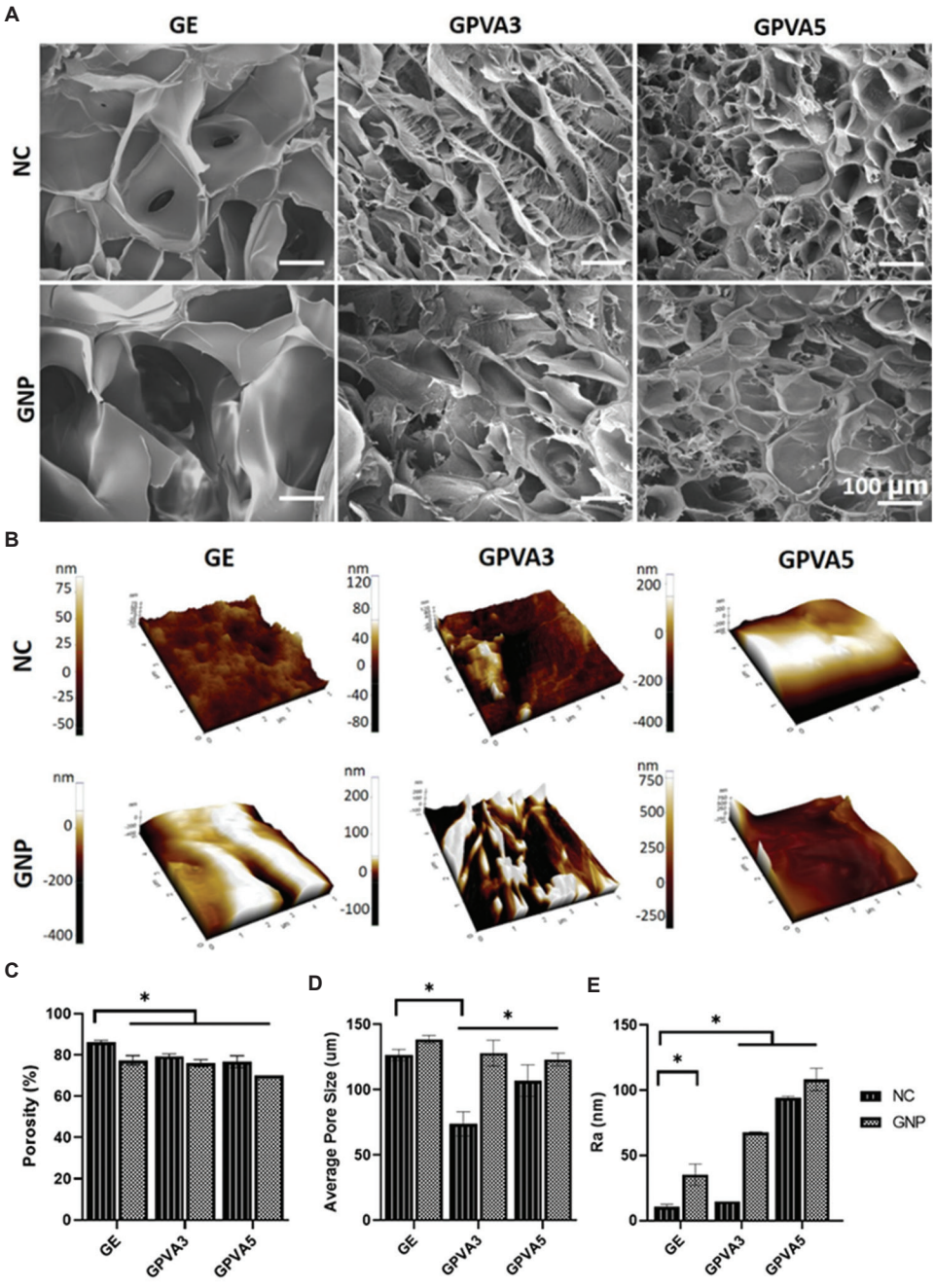

Figure 6. The evaluation of the microstructure analysis and surface roughness of the hydrogels. (A) Microstructure analysis through SEM under 100× magnification. (B) Surface roughness images through atomic force microscopy. (C) Porosity of hydrogels through liquid displacement method. (D) Average pore size of SEM photograph. (E) Surface roughness of the hydrogels. *$P < 0.05$.

hydrogels. Hydrogels with varying PVA concentration were initially examined for morphology using SEM in Figure 6A. The results demonstrated that both NC and GNP hydrogels have a porous structure with interconnected porosity with open and closed pores. Hydrogels with higher concentrations of PVA show smaller pore sizes. A high concentration of PVA in the polymer solution appears to impede the hydrogel from forming a homogeneous pore-like structure. The average pore sizes, as shown in Figure 6D, for GE_NC, GPVA3_NC, and GPVA5_NC are 123.69 ± 47.10 μm, 67.44 ± 22.20 μm, and 98.48 ± 28.55 μm, respectively. However, GE_GNP, GPVA3_GNP, and GPVA5_GNP (136.68 ± 63.31 μm, 121.62 ± 58.73 μm, and 119.59 ± 49.34 μm) have larger pore sizes with irregular structure as compared to NC hydrogels.

Moreover, Figure 6C presents the percentage of porosity of hydrogels. All of the hydrogels showed porosities ranging from 70% to 85%. The porosity of GPVA5_GNP was the lowest (71 ± 1.73%), whereas the porosity of GPVA3_GNP and GE_GNP was slightly increased (76 ± 1.73%, and 77 ± 2.30%). However, the porosity of GE_NC, GPVA3_NC, and GPVA5_NC is (86 ± 1%, 79.3 ± 1.15%, and 76.6 ± 2.89%), respectively.

3.7. Atomic force microscopy

Figure 6B shows 3D topography photographs of the surface roughness of the hydrogels. Figure 6E presents a summary of the acquired results. The surface roughness of hydrogels helps to maintain the cellular behavior and cell adhesion activity. The rough surface might cause the membranes to be highly hydrophobic. The surface roughness increased with an increase in the concentration of PVA in GPVA3_NC, GPVA3_GNP, GPVA5_NC, and GPVA5_GNP (14.79 ± 0.04 Ra, 67.57 ± 8.20 Ra, 94.26 ± 1.18 Ra, and 108.26 ± 8.58 Ra, respectively).

3.8. Cell viability

Biocompatibility of the 3D bioprinted GPVA hydrogels is an important aspect of any ECM-mimicking matrix. Fibroblasts play an essential role in wound healing primarily in the proliferative and remodeling stages. Figure 7A presents live/dead fluorescence staining images of printed HDFs after 24 h post-printing. Live cells were stained green, while dead cells were stained red. The HDFs were uniformly distributed over the 3D structure. The fluorescent pictures revealed no obvious morphological abnormalities, and there were no significant changes in the red fluorescence (dead cells) ratio between the groups. During the 1-day staining growth, the cells were all adherent, and morphologically, the cells maintained good growth, which was consistent for all hydrogels. However, according to Figure 7B, the cell viability decreased with the addition of PVA for GPVA3_GNP and GPVA5_GNP (93.5 ± 0.7% and 94.5 ± 0.7%, respectively). Moreover, as stated in Figure 7C, the printed bioinks have a cell attachment activity of 100%.

3.9. Proliferation of fibroblasts

The proliferation of fibroblasts encapsulated in the GE_GNP, GPVA3_GNP, and GPVA5_GNP was evaluated using MTT assay after 1, 5, and 7 days of incubation, as shown in Figure 7C. A significantly higher level of cell proliferation was observed in GPVA3_GNP formulation (108.95 ± 2.75%), followed by GPVA5_GNP (105.5 ± 2.12%) on day 7. As clearly shown in Figure 7C, after addition of PVA, the cell viability of HDFs that grew was greater than the cell viability in the GE_GNP. From day 1 until day 7, the HDFs were encapsulated in the bioinks never ceased to proliferate.

3.10. *In vitro* wound healing assay

An *in vitro* scratch wound experiment using human dermal fibroblasts (HDFs) cells was used to evaluate the effect of the gelatin-PVA biomaterial leachate media on wound healing. Sub-confluent or confluent HDFs were supplemented with biomaterial leachate media (GE_GNP, GPVA3_GNP, and GPVA5_GNP), and HDFs supplemented with full medium served as the positive control (Figure 7E). Further evaluation on wound healing progression is shown in Figure 7F, which presents a comparison of healing progress between the group treated with leachate media and the control group. A faster healing progression was observed in the GE_GNP, GPVA3_GNP, and GPV5_GNP (91.85 ± 1.76%, 98.67 ± 0.568%, and 99.67 ± 0.578%) after 72 h treatment with biomaterial leachate media. This shows that the rate of wound healing was significantly higher than the rate of healing in the control group, demonstrating the effectiveness of the GE_GNP, GPVA3_NP, and GPVA5_GNP in wound healing.

3.11. Cell morphology

The SEM images of cell culture within the bioink are shown in Figure 7D. The photomicrographs also reveal the growth, morphology, and spreading of HDFs within the matrix. The high-magnification images show that the HDFs seems attached to the base of the bioscaffold surface. The SEM images also show that the HDFs are in spherical cell shape rather than the normal morphology that was more elongated. The circular form of the HDFs implies that their lamellipodia or filopodia do not spread initially.

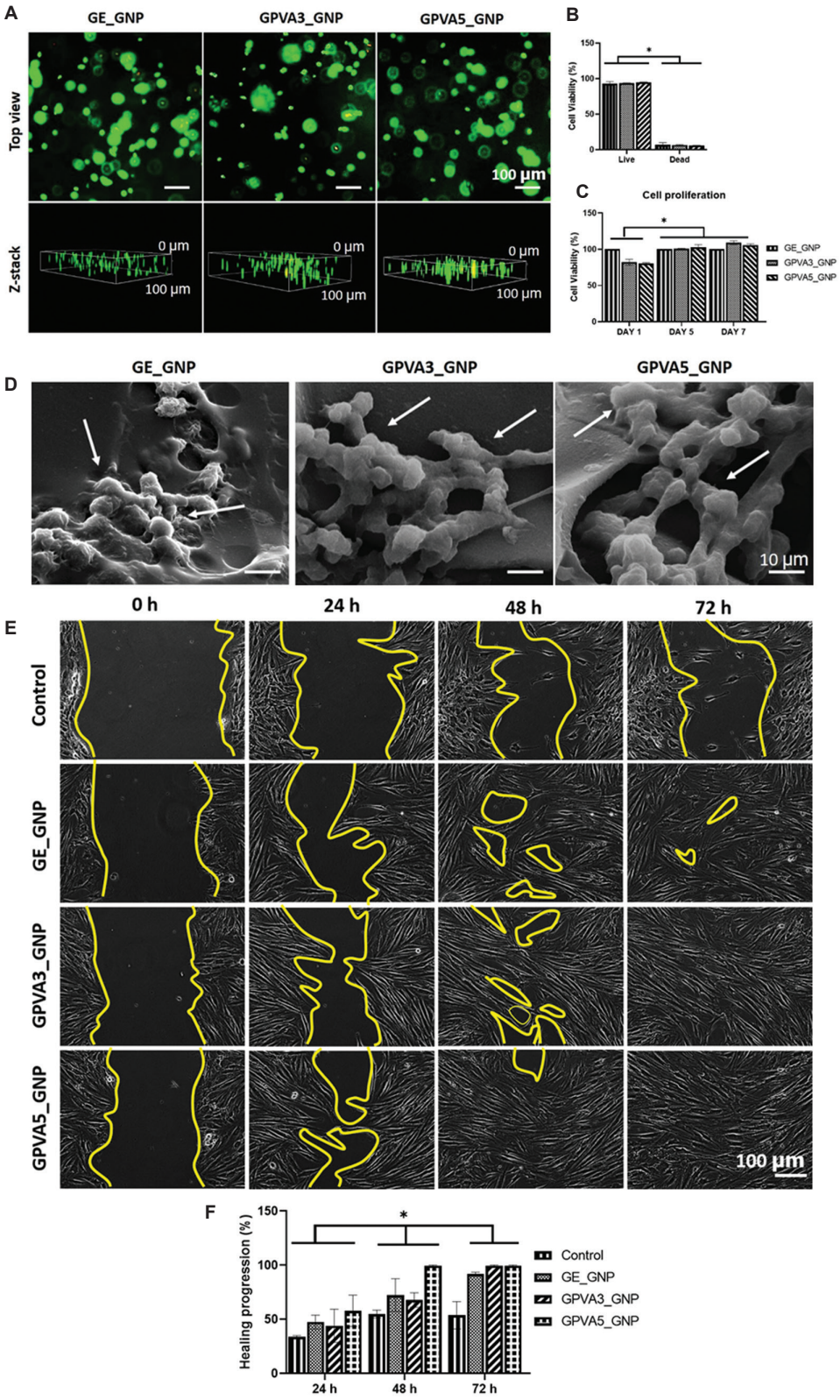

Figure 7. Cell-bioinks interaction. (A) Live/dead assay of HDFs. (B) Cell viability of the HDFs post-printing. (C) Cell proliferation activity. (D) SEM images show the cell morphology of HDFs in the bioink (scale bar, 10 µm). (E) Wound scratch assay of HDFs using leachate media for 72 h (scale bar, 100 µm). (F) Healing progression for wound scratch assay. *$P < 0.05$.

4. Discussion

Tissue engineering using 3D bioprinting technology help constructs biological structures that highly mimic native tissue. It is an authentic bioconvergence strategy before the establishment in future personalized or precision medicine applications. One of the main advantages of 3D bioprinting is the ability to include various bioinks or cell mixtures into specific spatial orientations or layers in the printed hydrogels[33]. In addition, this printing technology will enable live cells to react appropriately to the 3D-printed designs[34]. The revolutionary idea behind this biomatrix is to employ it as a one-time post-implantation cellular skin replacement. The hydrogels will progressively degrade on the injury site, followed by the regeneration of new tissue. Briefly, the encapsulation of cells in the bioinks with a layer-by-layer bioprinting concept is thought to encourage cell proliferation, accelerating the healing process. Therefore, this study aimed to use extrusion-based bioprinting technology to develop a functional cellular skin replacement that fits the intended wound shapes and sizes using the formulated bioinks composed of natural (GE) and synthetic-based polymers (PVA) crosslinked with GNP, a natural crosslinker.

4.1. Physical properties of hybrid bioinks

A printable biomaterial should have great printing resolution and excellent shape fidelity for irregular wound shape and facilitate surgeon handling. Brittle and soft hydrogel will limit surgical handling[35]. Moreover, the consistent flow of bioinks, which allows repeatable deposition of bioinks is a key feature of printed biomaterials[36]. In general, multiple deposition layers of bioinks will influence the geometrical accuracy and structural integrity. As more layers are stacked, the shape accuracy decreases as compared to a single layer of hydrogel. A previous investigation by De Stefano *et al.* on the multiple layers of bioinks depositions yielded the results similar to our findings, in which the shape fidelity of the multilayer hydrogels was significantly reduced by 6 layers of square printed grids compared to the single layer[37]. As a result, the printed filaments tended to collapse and merge between each other. Besides, a printable bioinks should have an optimum printing temperature and viscosity to preserve cell viability for extrusion-based bioprinting technique. Basically, the optimization of the printing temperature is depending on the viscosity of the hydrogels. Since the sol-gel temperature for gelatin-PVA is low, our study revealed the same findings as in previous studies by Chimene *et al.* and Shie *et al.*, in which they recommended that excellent structural fidelity could be achieved by printing the intended bioinks at room temperature (23 ± 2°C) as compared to 25 ± 2°C and 19 ± 2°C[38,39]. Moreover, our findings also can be supported by a previous study by Ding & Chang, which indicated that most of the bioinks were printed at the lower printing temperatures, and 23°C was selected as the most optimum printing temperature for the extrusion-based bioprinting[40]. In addition, low printing temperatures are required to extrude low-viscosity bioinks to allow consistent deposition of bioinks. In this study, the viscosity of the GPVA bioinks increased with the addition of PVA and crosslinker (GNP). This finding was similar to that in a previous study by Yang *et al.*, which showed that the addition of PVA significantly affects the viscosity of gelatin hydrogels, that is, the viscosity of the gelatin solution increased as the concentration of PVA increased[41]. Therefore, the addition of PVA and GNP into the bioinks was able to support the printability of the bioinks at room temperature.

Next, the physical properties were used to evaluate the performance of the desired hydrogel. Developing a biodegradable hydrogel for wound healing application is highly desired to allow it to be degraded at an appropriate timeline following new tissue regeneration. Since rapid wound closure is necessary to prevent infection, the designated hydrogels must not be degraded for at least 14 days before wound healing applications in the *in vivo* model[42]. A study by Zandi *et al.* suggested that *in vivo* models could achieve 90% wound closure after treatment with bioscaffolds for 2 weeks[43]. The GPVA hydrogels possessed an acceptable biodegradation rate for future wound healing applications. For comparison, crosslinked gelatin hydrogels with the addition of PVA enable prolonged durability as compared to GE_GNP hydrogel only. This finding was similar with a previous study by Hezaveh & Muhamad, which indicated that utilizing genipin in the hydrogels can prevent it from bursting in order to control its durability[44]. Thus, raising the concentration of PVA and crosslinker will slow down the biodegradation rate of the hydrogels at the injury site. In addition, a previous study by Mahnama *et al.* has proven that gelatin hydrogels incorporated with PVA in higher ratio have the slowest biodegradation rate after 27 days[45].

Besides, in wound healing application, one of the characteristics that contributed to the skin's barrier function is surface wettability. The hydrophilic properties of the hydrogels were confirmed through contact angle analysis, which showed that all printed GPVA hydrogels possessed hydrophilic properties that may be caused by the hydrophilic nature of gelatin and PVA polymer. However, the incorporation of PVA into gelatin hydrogels reduced the hydrophilicity of the printed hydrogels. This finding was similar with a previous study by Cheng *et al.*, which indicated that the hydrophilicity of the gelatin-PVA hydrogels was relatively lower than gelatin hydrogels[46]. Hydrophilicity of bioinks is a crucial characteristic that

provides a desirable property to enhance cellular activities and influence the moisture of the printed hydrogels. A moist environment promotes wound healing by enabling the encapsulated cells to migrate freely through the hydrogels that are often present in wound exudate[47]. Moreover, the previous studies by Zidaric *et al.* suggested that the hydrophilicity and viscosity of the bioinks solution have a significant impact on the printing accuracy and live cell encapsulation[47]. Consequently, hydrophobic bioinks prevent the bioinks from spreading well during printing[48].

Next, an ideal skin substitute is characterized by an optimum water uptake capacity through swelling ratio. A study by Agubata *et al.* suggested that a hydrogel candidate for wound healing applications should have a water holding capacity of about 500%, as this will prevent exudates from accumulating in the wound area[49]. This finding was similar with our swelling ratio results that were considered fit for wound healing application as it has >500% of swelling ratio. However, the swelling ratio decreased in the presence of PVA in the hydrogels. This finding was comparable with a previous study on the gelatin-PVA hydrogels by Jeong *et al.*, which indicated that the swelling ratio decreased when the concentration of PVA increased[50]. This phenomenon occurred due to the formation of covalent bonds between the functional groups of the gelatin and PVA, which might cause smaller pore sizes[50]. In addition, an ideal WVTR might keep skin at the proper degree of moisture and could prevent dryness or maceration from damaging a wound by regulating the moisture of the microenvironment[51]. In this study, the crosslinked hydrogels have WVTR in the range of 700–1200 g/m^2/h, which was ideal for rapid wound recovery. This finding is similar with the previous studies by Sutar *et al.* and Lou, which indicated the normal WVTR for normal skin was 204 g/m^2/24 h while for injured skin was 279 g/m^2/24 h[52,53]. Moreover, the literature also claims that human skin transpires water vapor at a rate of between 240 and 1920 g/m^2 every 24 h[54].

4.2. Dual-functions of genipin on hybrid bioinks development

Besides, degree of crosslinking was another criterion considered for skin application. Crosslinking of the hydrogel has been shown to be an effective method for enhancing both the mechanical and thermal properties of the hydrogels. As the gels successfully crosslinked with the genipin (GNP), the hydrogels turned blue. This is because the hydrogel network contains amino groups, causing GNP to interact with the hydrogels. As a result, this phenomenon occurs. Moreover, the results of this investigation are consistent with other study by Butler *et al.*, which indicated that the polymerization of genipin by oxygen radicals results in the formation of a blue pigment[55]. After being crosslinked with 0.1% of GNP, the degree of crosslinking findings revealed that the hydrogels had a crosslinking level of >40%. Arif *et al.*, who studied the effects of 0.1% GNP crosslinking on the gelatin hydrogel, also found that the hydrogels have roughly a crosslinking degree of 39%[56]. It was found that without crosslinking, gelatin hydrogels will have poor shape stability and mechanical strength, thereby limiting their biomedical applications[57].

Moreover, genipin is preferable over other crosslinkers not only because it functions as a crosslinker, but also because of its biological activities, including anti-inflammatory and antioxidant properties that are produced by the GNP[58]. Continuous inflammation, pathogen infection, and oxidative stress are a few variables that might adversely influence the healing process of wounds. The antioxidant properties of the hydrogels were determined by measuring the free radical scavenging activity through DPPH and ABTS assay. After crosslinked with GNP, the hydrogels have been shown to have a scavenging activity of >25%, as shown in Figure 3F and G. Since 0.1% of GNP was employed in this research, it might have antioxidant effects that maintain cell proliferation activity. Notably, a significant finding by Kim *et al.* found that higher dosages of GNP would increase the quantity of reactive oxygen species (ROS) and induce cytotoxicity, whereas only low doses of GNP will have antioxidant properties[59]. Moreover, Fan *et al.* found that GNP seems to activate numerous key genes encoding antioxidant and xenobiotic-metabolizing enzymes[60]. Due to its antioxidant characteristics, genipin has been explored as a possible cancer treatment[61]. On the other hand, a comparison research carried out by Zulkiflee & Fauzi found that gelatin and PVA polymers do not have any antioxidant characteristics, unless additional antioxidant components are included[14].

4.3. Hybrid bioinks printability through extrusion-based bioprinting

Viscosity of bioinks is crucial for extrusion-based bioprinting. Moreover, the hydrogels' shear-thinning properties rely on the viscosity of the bioinks[16]. Higher viscosity of bioinks will clog the dispensing nozzle during extrusion, while lower viscosity of bioinks will cause extruded filaments to overspread and collapse[62]. According to our finding, the viscosity of gelatin bioinks increased with the addition of PVA and crosslinker. A previous study by Tung *et al.* suggested that the viscosity remained more stable with higher PVA content, preserving the usual pseudoplastic behavior of hydrogels[63], and Masri *et al.* reported the similar finding in which the viscosity of the gelatin hydrogel increased with the addition of genipin and PVA[64]. On the other hand, the storage modulus (G') of hydrogels with varying viscosities was measured to

determine the interaction of PVA and crosslinker with gelatin hydrogel. In this research, the G' steadily drops at low frequencies until it reaches a minimum at a certain frequency, at which point the modulus rises. The addition of PVA did not increase the elasticity of the gelatin hydrogel. This finding is correlated with a study by Moraes *et al.*, which indicated that gelatin and PVA polymers practically did not exhibit elastic behavior (G') and also did not exhibit any phase change within the temperature range investigated[65]. Besides, another finding on the viscoelasticity of the gelatin-PVA hydrogel was found by Gelli *et al.*, who reported that the incorporation of PVA into gelatin hydrogels decreased in the storage modulus[66]. Moreover, the progression of stiffening and gel structure is confirmed by the increasing rate of G' which is higher than that of loss modulus (G").

The crystallinity pattern of the gelatin-PVA hydrogels was evaluated using XRD, as shown in Figure 5A. Since gelatin is a semi-crystalline polymer, there is a broad peak in the range 10–25° (2θ) for all hydrogels. The gelatin-PVA hydrogels have the highest peak at (2θ) 19.5° and this finding matches a previous study by Zandraa *et al.*[67] Following the incorporation of gelatin with PVA in the hydrogels, the crystallinity level was slightly reduced (Table 1). This occurrence was described by Swaroop *et al.*, claiming that the regularity of gelatin was disrupted by intermolecular contact[68]. Similar results were obtained in a recent work by Zulkiflee & Fauzi, which described how the addition of PVA to gelatin hydrogel would decrease crystallinity[14]. In addition, following crosslinking with genipin, the crystallinity of crosslinked gelatin-PVA hydrogels increased in comparison to non-crosslinked hydrogels. This result was highly similar to a recent work by Zawani *et al.*, which produced similar outcomes following genipin crosslinking of the hydrogels[69].

Besides, the interaction between polymers and functional groups of the hydrogels was characterized using FTIR. Based on Figure 4B, both crosslinked and non-crosslinked hydrogels exhibited distinct spectra in the region of 2750 – 3500 cm^{-1}. GE_NC hydrogels showed vibration of C-H stretching that appeared at wavenumbers 2934.3 and 3301.98 cm^{-1} that represent Amide A and Amide B. The hydroxyl groups (O-H) stretching in the GPVA hydrogels showed a broad peak in the 2900 – 3500 cm^{-1}. This result was consistent with a previous study by Thangprasert *et al.*, which demonstrated that the hydroxyl group stretching formation was initiated by the interaction of intramolecular and intermolecular hydrogen bonds between GE and PVA[70]. In contrast, hydrogels with greater PVA concentrations exhibited a stronger absorption peak. Moreover, the bands from 1200 to 1700 cm^{-1} in all hydrogels were related to the formation of amine (C-N) I, II, and III due to the interaction of amine groups of GE with GNP. It was demonstrated that the gelatin-PVA hydrogels did not present any extra peaks in a way that implies that 3D bioprinting approach did not contribute to any unfavorable chemical interactions.

4.4. Bioinks 3D microstructure and cellular compatibility

An appropriate porosity of skin substitute is crucial for wound healing application to allow efficient deposition of ECM, and promote cell migration activity and tissue integration. SEM was used to determine the microporous structures of the 3D-printed hydrogels. The interconnected pores were visible in all hydrogel groups and average pore sizes were calculated to be greater than 100 μm. A previous study by Yannas *et al.* suggested that 20 – 125 m should be the ideal pore size for reconstructing adult skin[71]. Moreover, GE_GNP demonstrated to have the biggest pore sizes among the crosslinked groups. The addition of PVA to the gelatin hydrogels reduced their porosity. This result was similar with a previous finding by Thangprasert *et al.* and Labus and Radosinski, which indicated that the pore diameters of gelatin hydrogel were reduced and substantially smaller by adding PVA to the gelatin hydrogels[70,72]. These results occurred due to the penetration of PVA molecules into the open spaces between gelatin chains. Moreover, the addition of GNP affected the pore diameters of gelatin-PVA hydrogels due to the formation of covalent bond. The number of tiny pores increased in the crosslinked polymer chains in the interpenetrating hydrogel as compared to the non-crosslinked hydrogels. A previous study by Erdag *et al.* showed that samples with lower GNP concentrations had a higher number of tiny pores as compared to the samples with higher GNP concentrations[73]. Thus, our formulations might be able to aid in absorbing wound exudate, lower the risk of infection, and provide a conducive environment that promotes faster wound healing due to the presence of appropriate porosity.

Cell response to a toxicant or new substances and the measurement of cell viability are well known as key aspects in toxicity testing. The extrusion-based bioprinting technique exhibited no sign of cell membrane damage after printing. The addition of different concentration of PVA (3% and 5%) and crosslinker (GNP) to the gelatin hydrogels clearly demonstrated that no obvious cell morphological changes occurred after they were encapsulated in the bioinks. The live/dead assay revealed that nearly all the HDFs were stained green and still alive after bioprinting. Thus, our results demonstrated that all hydrogels could sustain high cell viability (>90%) after 24-h extrusion, indicating that the bioinks are biocompatible and less toxic

toward HDFs. This discovery is confirmed by Barba *et al.* and Masri *et al.*, who discovered that both gelatin and PVA are biocompatible to HDFs, with cell viability of >88%, evaluated on gelatin and PVA hydrogels[64,74]. Furthermore, the live/dead assay that measures the cell proliferation activity revealed that the gelatin-PVA bioinks were able to support HDFs proliferation and offered a conducive environment for cell growth. Besides, an *in vitro* wound scratch assay was performed to evaluate the migration activity of the HDFs for future wound healing application. The results in Figure 7E demonstrated that both gelatin and gelatin-PVA hydrogels indicated an efficient cell migration activity after 72-h exposure to the hydrogel's leachate media. The cell monolayer scratch was partially closed after 24 h and fully closed after 72 h of leachate treatments as compared to the controls. A similar finding was observed in a previous study by George *et al.*, which indicated that the cell monolayers moved toward the opening of the scratch region and partially closed after treatment with biomaterial leachate for 24 h[75].

Gelatin-PVA scaffolds with particular ratios can mimic natural tissues for cell adhesion and growth. However, a study by Kakarla *et al.* found that the higher PVA concentrations in the hydrogel may reduce HDFs growth[76]. Besides, due to PVA's lack of cell adhesion sites, larger amounts may limit cell attachment. This finding can be confirmed by a previous study on pure PVA by Jeong *et al.*, which found no cell adhesion activity due to the absence of ligands bound to cell-surface receptors[50]. However, there was no distinct difference on cell attachment activity between gelatin and gelatin-PVA hydrogels. In addition, the morphological structure of cells was observed using SEM after encapsulated in the bioinks. Figure 7D demonstrates that the HDFs emerged as small spherical forms and were evenly distributed on the surface of the gelatin-PVA hydrogels. Moreover, Thangprasert *et al.* and Yannas *et al.* reported similar results for the morphological structure of encapsulated cells in bioinks with spherical-shaped cells and maintained cell viability in different types of hydrogels after days 5 and 7[70,71]. According to the findings by Crosby *et al.*, HDFs have an expanded morphology in softer hydrogels and appear as rounded/spherical shapes in stiffer hydrogels[77].

5. Conclusion

GPVA bioinks were successfully fabricated using extrusion-based bioprinting with promising printability at optimum printing temperature (23 ± 2°C). The addition of PVA increased the viscosity of the bioinks; therefore, a hydrogel construct with better shape fidelity is more printable. In addition, the constructed bioinks, as cellular skin replacement, also exhibit excellent physicochemical properties based on their swelling characteristics. The composite bioinks demonstrated excellent fluid absorption capacity with hydrophilic properties. The addition of PVA developed biostable rheological properties for the bioinks without impairing the printability and *in vitro* testing towards HDFs. The *in vitro* cytotoxicity testing through live/dead staining showed that the addition of PVA resulted in excellent cell viability after bioprinting. The GPVA bioinks thus demonstrated outstanding physicochemical and rheological qualities and satisfied all criteria for suitable medical applications. As a result, it has good physical and forming qualities, making it as a potential cellular skin replacement.

Acknowledgments

All authors would like to express immense gratitude to the Faculty of Medicine, UKM for the guidance and resources to complete this manuscript. This study has been performed under good quality management of ISO 9001:2015 for research facilities.

Funding

The study was funded by Ministry of Higher Education (MoHE) under the Skim Geran Penyelidikan Fundamental (FRGS), grant code: FRGS/1/2020/STG05/UKM/02/7.

Conflict of interest

The authors declare no conflict of interest.

Author contributions

Conceptualization: Syafira Masri, Ruszymah Idrus, Mh Busra Fauzi

Investigation: Syafira Masri, Izhar Abd Aziz, Mh Busra Fauzi

Methodology: Syafira Masri, Manira Maarof, Mh Busra Fauzi

Formal analysis: Syafira Masri

Writing – original draft: Syafira Masri

Writing – review & editing: Syafira Masri, Manira Maarof, Ruszymah Idrus, Mh Busra Fauzi.

Ethics approval and consent to participate

The study design was approved by the Universiti Kebangsaan Malaysia Research Ethics Committee (Code no. FF-2021-376 and JEP-2021-605).

Consent for publication

The human skin samples were obtained from six consented patients (written and verbal) and permission was obtained from each of the subjects to publish their data.

Availability of data

Not applicable.

References

1. Wei C, Feng Y, Che D, *et al.*, 2021, Biomaterials in skin tissue engineering. *Int J Polym Mater Polym Biomater*, 71: 1–19.

   https://doi.org/10.1080/00914037.2021.1933977

2. Fadilah NI, Jailani MS, Hisham MA, *et al.*, 2022, Cell secretomes for wound healing and tissue regeneration : Next generation acellular based tissue engineered products. *J Tissue Eng*, 13: 20417314221114273.

   https://doi.org/10.1177/20417314221114273

3. Weng T, Zhang W, Xia Y, *et al.*, 2021, 3D bioprinting for skin tissue engineering: Current status and perspectives. *J Tissue Eng*, 12: 20417314211028574.

   https://doi.org/10.1177/20417314211028574

4. Rodrigues M, Kosaric N, Bonham CA, *et al.*, 2019, Wound healing: A cellular perspective. *Physiol Rev*, 99: 665–706.

   https://doi.org/10.1152/physrev.00067.2017

5. Luo R, Dai J, Zhang J, *et al.*, 2021, Accelerated skin wound healing by electrical stimulation. *Adv Healthc Mater*, 10: 1–15.

   https://doi.org/10.1002/adhm.202100557

6. Zeng R, Lin C, Lin Z, *et al.*, 2018, Approaches to cutaneous wound healing: Basics and future directions. *Cell Tissue Res*, 374: 217–232.

   https://doi.org/10.1007/s00441-018-2830-1

7. Zawani M, Fauzi MB, 2021, Injectable hydrogels for chronic skin wound management: A concise review. *Biomedicines*, 9: 527.

   https://doi.org/10.3390/biomedicines9050527

8. Kang JI, Park KM, Kang, 2021, Advances in gelatin-based hydrogels for wound management. *J Mater Chem B*, 9: 1503–1520.

   https://doi.org/10.1039/d0tb02582h

9. Sen CK, 2021, Human wound and its burden: Updated 2020 compendium of estimates. *Adv Wound Care (New Rochelle)*, 10: 281–292.

   https://doi.org/10.1089/wound.2021.0026

10. Masri S, Zawani M, Zulkiflee I, *et al.*, 2022, Cellular interaction of human skin cells towards natural bioink via 3d-bioprinting technologies for chronic wound: A comprehensive review. *Int J Mol Sci*, 23: 476.

    https://doi.org/10.3390/ijms23010476

11. Fuchs C, Pham L, Wang Y, *et al.*, 2021, MagneTEskin-reconstructing skin by magnetically induced assembly of autologous microtissue cores. *Sci Adv*, 7: 1–11.

    https://doi.org/10.1126/sciadv.abj0864

12. Boyce ST, Lalley AL, 2018, Tissue engineering of skin and regenerative medicine for wound care. *Burns Trauma*, 6: 4.

    https://doi.org/10.1186/s41038-017-0103-y

13. Salleh A, Mustafa N, Teow TH, *et al.*, 2022, Dual-layered approach of ovine collagen-gelatin/cellulose hybrid biomatrix containing graphene oxide-silver nanoparticles for cutaneous wound healing : Fabrication, physicochemical, cytotoxicity and, antibacterial characterisation. *Biomedicines*, 10: 816.

14. Zulkiflee I, Fauzi MB, 2021, Gelatin-polyvinyl alcohol film for tissue engineering: A concise review. *Biomedicines*, 9: 979.

    https://doi.org/10.3390/biomedicines9080979

15. Roy R, Tiwari M, Donelli G, *et al.*, 2018, Strategies for combating bacterial biofilms: A focus on anti-biofilm agents and their mechanisms of action. *Virulence*, 9: 522–554.

    https://doi.org/10.1080/21505594.2017.1313372

16. Masri S, Fauzi MB, 2021, Current insight of printability quality improvement strategies in natural-based bioinks for skin regeneration and wound healing. *Polymers (Basel)*, 13: 1011.

    https://doi.org/10.3390/polym13071011

17. Koch F, Wehrle M, Tröndle K, *et al.*, 2019, Rapid Assessment of Combined Drop on Demand and Extrusion-based Bioprinting with Controlled Shear Stress and High Shape Fidelity. In: 2019 20th International Conference Solid-State Sensors, Actuators Microsystems Eurosensors XXXIII, Transducers 2019 Eurosensors XXXIII. Germany, IEEE. p1048–1051.

    https://doi.org/10.1109/TRANSDUCERS.2019.8808595

18. He P, Zhao J, Zhang J, *et al.*, 2018, Bioprinting of skin constructs for wound healing. *Burns Trauma*, 6: 1–10.

    https://doi.org/10.1186/s41038-017-0104-x

19. Ghosh S, Kaushik G, Roy P, *et al.*, 2021, Application of 3D bioprinting in wound healing: A review. *Trends Biomater Artif Organs*, 35: 495–509.

20. Wang Y, Yuan X, Yao B, *et al.*, 2022, Tailoring bioinks of extrusion-based bioprinting for cutaneous wound healing. *Bioact Mater*, 17: 178–194.

    https://doi.org/10.1016/j.bioactmat.2022.01.024

21. Wang X, Ao Q, Tian X, *et al.*, 2017, Gelatin-based hydrogels for organ 3D bioprinting. *Polymers (Basel)*, 9: 401.

    https://doi.org/10.3390/polym9090401

22. Young S, Wong ME, Tabata Y, *et al.*, 2005, Gelatin as a delivery vehicle for the controlled release of bioactive molecules. *J Control Release*, 109: 256–274.

    https://doi.org/10.1016/j.jconrel.2005.09.023

23. Badylak SF, Freytes DO, Gilbert TW, 2009, Extracellular matrix as a biological scaffold material: Structure and function. *Acta Biomater*, 5: 1–13.

https://doi.org/10.1016/j.actbio.2008.09.013

24. Huang CY, Hu KH, Wei ZH, 2016, Comparison of cell behavior on pva/pva-gelatin electrospun nanofibers with random and aligned configuration. *Sci Rep*, 6: 37960.

https://doi.org/10.1038/srep37960

25. Nguyen TH, Ventura R, Min YK, *et al*., 2016, Genipin cross-linked polyvinyl alcohol-gelatin hydrogel for bone regeneration. *J Biomed Sci Eng*, 9: 419–429.

https://doi.org/10.4236/jbise.2016.99037

26. Bedran-Russo AK, Pereira PN, Duarte WR, *et al*., 2007, Application of crosslinkers to dentin collagen enhances the ultimate tensile strength. *J Biomed Mater Res Part B Appl Biomater*, 80: 268–272.

https://doi.org/10.1002/jbm.b.30593

27. Fernandes DM, Barbosaa WS, Rangel WS, *et al*., 2021, Polymeric membrane based on polyactic acid and babassu oil for wound healing. *Mater Today Commun*, 26: 102173.

https://doi.org/10.1016/j.mtcomm.2021.102173

28. Ghaffari R, Salimi-Kenari H, Fahimipour F, *et al*., 2020, Fabrication and characterization of dextran/nanocrystalline β-tricalcium phosphate nanocomposite hydrogel scaffolds. *Int J Biol Macromol*, 148: 434–448.

https://doi.org/10.1016/j.ijbiomac.2020.01.112

29. Fauzi MB, Lokanathan Y, Nadzir MM, *et al*., 2017, Attachment, proliferation, and morphological properties of human dermal fibroblasts on ovine tendon collagen scaffolds: A comparative study. *Malaysian J Med Sci*, 24: 33–43.

https://doi.org/10.21315/mjms2017.24.2.5

30. Maver T, Hribernik S, Mohan T, *et al*., 2015, Functional wound dressing materials with highly tunable drug release properties. *RSC Adv*, 5: 77873–77884.

https://doi.org/10.1039/C5RA11972C

31. Rodríguez-Rodríguez R, García-Carvajal ZY, Jiménez-Palomar I, *et al*., 2019, Development of gelatin/chitosan/PVA hydrogels: Thermal stability, water state, viscoelasticity, and cytotoxicity assays. *J Appl Polym Sci*, 136: 1–9.

https://doi.org/10.1002/app.47149

32. Ghanbari M, Salavati-Niasari M, Mohandes F, 2021, Injectable hydrogels based on oxidized alginate-gelatin reinforced by carbon nitride quantum dots for tissue engineering. *Int J Pharm*, 602: 120660.

https://doi.org/10.1016/j.ijpharm.2021.120660

33. Tan CT, Liang K, Ngo ZH, *et al*., 2020, Application of 3D bioprinting technologies to the management and treatment of diabetic foot ulcers. *Biomedicines*, 8: 441.

https://doi.org/10.3390/biomedicines8100441

34. Huang S, Yao B, Xie J, *et al*., 2016, 3D bioprinted extracellular matrix mimics facilitate directed differentiation of epithelial progenitors for sweat gland regeneration. *Acta Biomater*, 32: 170–177.

https://doi.org/10.1016/j.actbio.2015.12.039

35. He B, Wang J, Xie M, *et al*., 2022, 3D printed biomimetic epithelium/stroma bilayer hydrogel implant for corneal regeneration. *Bioact Mater*, 17: 234–247.

https://doi.org/10.1016/j.bioactmat.2022.01.034

36. Rodríguez-rodríguez R, Espinosa-andrews H, Velasquillo-Martínez C, *et al*., 2020, Composite hydrogels based on gelatin, chitosan and polyvinyl alcohol to biomedical applications : A review. *Int J Polym Mater Polym Biomater*, 69: 1–20.

https://doi.org/10.1080/00914037.2019.1581780

37. De Stefano P, Briatico-Vangosa F, Bianchi E, *et al*., 2021, Bioprinting of matrigel scaffolds for cancer research. *Polymers (Basel)*, 13: 2026.

https://doi.org/10.3390/polym13122026

38. Chimene D, Lennox KK, Kaunas RR, *et al*., 2016, Advanced bioinks for 3D printing: A materials science perspective. *Ann Biomed Eng*, 44: 2090–2102.

https://doi.org/10.1007/s10439-016-1638-y

39. Shie MY, Lee JJ, Ho CC, *et al*., 2020, Effects of gelatin methacrylate bio-ink concentration on mechano-physical properties and human dermal. *Polymers (Basel)*, 2: 1930.

https://doi.org/10.3390/polym12091930

40. Ding H, Chang RC, 2018, Printability study of bioprinted tubular structures using liquid hydrogel precursors in a support bath. *Appl Sci*, 8: 403.

https://doi.org/10.3390/app8030403

41. Yang D, Li Y, Nie J, 2007, Preparation of gelatin/PVA nanofibers and their potential application in controlled release of drugs. *Carbohydr Polym*, 69: 538–543.

https://doi.org/10.1016/j.carbpol.2007.01.008

42. Sgonc R, Gruber J, 2013, Age-related aspects of cutaneous wound healing: A mini-review. *Gerontology*, 59: 159–164.

https://doi.org/10.1159/000342344

43. Zandi N, Dolatyar B, Lotfi R, *et al*., 2021, Biomimetic nanoengineered scaffold for enhanced full-thickness cutaneous wound healing. *Acta Biomater*, 124: 191–204.

https://doi.org/10.1016/j.actbio.2021.01.029

44. Hezaveh H, Muhamad II, 2013, Controlled drug release via minimization of burst release in pH-response kappa-carrageenan/polyvinyl alcohol hydrogels. *Chem Eng Res Des*, 91: 508–519.

https://doi.org/10.1016/j.cherd.2012.08.014

45. Mahnama H, Dadbin S, Frounchi M, *et al*., 2017, Preparation of biodegradable gelatin/PVA porous scaffolds for skin regeneration. *Artif Cells Nanomed Biotechnol*, 45: 928–935.

https://doi.org/10.1080/21691401.2016.1193025

46. Cheng L, Zou Q, Zou L, *et al*., 2013, Properties of vanillin modified poly(vinyl alcohol)/gelatin composite. *Appl Mech Mater*, 327: 48–52.

https://doi.org/10.4028/www.scientific.net/AMM.327.48

47. Zidaric T, Milojevic M, Gradisnik L, *et al*., 2020, Polysaccharide-based bioink formulation for 3D bioprinting of an *in vitro* model of the human dermis. *Nanomaterials*, 10: 733.

https://doi.org/10.3390/nano10040733

48. Naghieh S, Chen X, 2021, Printability-A key issue in extrusion-based bioprinting. *J Pharm Anal*, 11: 564–579.

https://doi.org/10.1016/j.jpha.2021.02.001

49. Agubata CO, Mbah MA, Akpa PA, *et al*., 2021, Application of self-healing, swellable and biodegradable polymers for wound treatment. *J Wound Care*, 30: IVI–IVX.

https://doi.org/10.12968/jowc.2021.30.Sup9a.IV

50. Jeong H, Lee DY, Yang DH, *et al*., 2022, Mechanical and cell-adhesive properties of gelatin/polyvinyl alcohol hydrogels and their application in wound dressing. *Macromol Res*, 30: 223–229.

https://doi.org/10.1007/s13233-022-0027-7

51. Xu R, Xia H, He W, *et al*., 2016, Controlled water vapor transmission rate promotes wound-healing via wound re-epithelialization and contraction enhancement. *Sci Rep*, 6: 1–12.

https://doi.org/10.1038/srep24596

52. Sutar T, Bangde P, Dandekar P, *et al*., 2021, Fabrication of herbal hemostat films loaded with medicinal tridax procumbenns extracts. *Fibers Polym*, 22: 2135–2144.

https://doi.org/10.1007/s12221-021-0808-1

53. Lou CW, 2008, Process technology and properties evaluation of a chitosan-coated tencel/cotton nonwoven fabric as a wound dressing. *Fibers Polym*, 9: 286–292.

https://doi.org/10.1007/s12221-008-0046-9

54. Gu Z, Xie H, Huang C, *et al*., 2013, Preparation of chitosan/silk fibroin blending membrane fixed with alginate dialdehyde for wound dressing. *Int J Biol Macromol*, 58: 121–126.

https://doi.org/10.1016/j.ijbiomac.2013.03.059

55. Butler MF, Ng YF, Pudney PD, 2003, Mechanism and kinetics of the crosslinking reaction between biopolymers containing primary amine groups and genipin. *J Polym Sci Part A Polym Chem*, 41: 3941–3953.

https://doi.org/10.1002/pola.10960

56. Arif MM, Fauzi MB, Nordin A, *et al*., 2020, Fabrication of bio-based gelatin sponge for potential use as a functional acellular skin substitute. *Polymers (Basel)*, 12: 1–19.

https://doi.org/10.3390/polym12112678

57. Wang QS, Wang GF, Zhang HY, *et al*., 2021, Development of genipin crosslinked gelatin matrices on surface interaction: Enhancing the biocompatibility by attenuating sterile inflammation. *Chin J Chem Eng*, 38: 205–215.

https://doi.org/10.1016/j.cjche.2021.03.022

58. Nike DU, Fadilah NI, Sallehuddin N, *et al*., 2022, Genipin-crosslinking effects on biomatrix development for cutaneous wound healing: A concise review. *Front Bioeng Biotechnol*, 10: 1–16.

https://doi.org/10.3389/fbioe.2022.865014

59. Kim JM, Ko H, Kim SJ, *et al*., 2016, Chemopreventive properties of genipin on AGS cell line via induction of JNK/Nrf2/ARE signaling pathway. *J Biochem Mol Toxicol*, 30: 45–54.

https://doi.org/10.1002/jbt.21741

60. Fan X, Lin L, Cui B, *et al*., 2020, Therapeutic potential of genipin in various acute liver injury, fulminant hepatitis, NAFLD and other non-cancer liver diseases: More friend than foe. *Pharmacol Res*, 159: 104945.

https://doi.org/10.1016/j.phrs.2020.104945

61. Naseriyeh T, Noori T, Zhaleh H, *et al*., 2022, Enhanced *in vitro* cytotoxicity and intracellular uptake of genipin via loaded on nano-liposomes made from soybean lecithin in MCF-7 cells. *Nanomed J*, 9: 67–76.

https://doi.org/10.22038/NMJ.2022.60524.1626

62. El-Habashy SE, El-Kamel AH, Essawy MM, *et al*., 2021, Engineering 3D-printed core-shell hydrogel scaffolds reinforced with hybrid hydroxyapatite/polycaprolactone nanoparticles for *in vivo* bone regeneration. *Biomater Sci*, 9: 4019–4039.

https://doi.org/10.1039/d1bm00062d

63. Tung NT, Vu VD, Nguyen PL, 2019, DoE-based development, physicochemical characterization, and pharmacological evaluation of a topical hydrogel containing betamethasone dipropionate microemulsion. *Colloids Surf B Biointerfaces*, 181: 480–488.

https://doi.org/10.1016/j.colsurfb.2019.06.002

64. Masri S, Maarof M, Mohd NF, *et al*., 2022, Injectable crosslinked genipin hybrid gelatin-PVA hydrogels for future use as bioinks in expediting cutaneous healing capacity : Physicochemical characterisation and cytotoxicity evaluation. *Biomedicine*, 10: 2651.

https://doi.org/10.3390/biomedicines10102651

65. Moraes IC, Carvalho RA, Bittante AM, *et al*., 2009, Film forming solutions based on gelatin and poly(vinyl alcohol)

blends: Thermal and rheological characterizations. *J Food Eng*, 95: 588–596.

https://doi.org/10.1016/j.jfoodeng.2009.06.023

66. Gelli R, Del Buffa S, Tempesti P, *et al*., 2017, Multi-scale investigation of gelatin/poly(vinyl alcohol) interactions in water. *Colloids Surf A Physicochem Eng Asp*, 532: 18–25.

https://doi.org/10.1016/j.colsurfa.2017.07.049

67. Zandraa O, Ngwabebhoh FA, Patwa R, *et al*., 2021, Development of dual crosslinked mumio-based hydrogel dressing for wound healing application: Physico-chemistry and antimicrobial activity. *Int J Pharm*, 607: 120952.

https://doi.org/10.1016/j.ijpharm.2021.120952

68. Swaroop K, Gaana MJ, Shruthi SS, *et al*., 2019, Studies on swelling behaviour of radiolytically synthesised PVA/gelatin hydrogels. *AIP Conf Proc*, 2115: 030050.

https://doi.org/10.1063/1.5112889

69. Zawani M, Maarof M, Tabata Y, *et al*., 2022, Quercetin-embedded gelastin injectable hydrogel as provisional biotemplate for future cutaneous application: Optimization and *in vitro* evaluation. *Gels*, 8: 623.

https://doi.org/10.3390/gels8100623

70. Thangprasert A, Tansakul C, Thuaksubun N, *et al*., 2019, Mimicked hybrid hydrogel based on gelatin/PVA for tissue engineering in subchondral bone interface for osteoarthritis surgery. *Mater Des*, 183: 108113.

https://doi.org/10.1016/j.matdes.2019.108113

71. Yannas IV, Lee E, Orgill DP, *et al*., 1989, Synthesis and characterization of a model extracellular matrix that induces partial regeneration of adult mammalian skin. *Proc Natl Acad Sci USA*, 86: 933–937.

72. Labus K, Radosinski L, Kotowski P, 2021, Functional properties of two-component hydrogel systems based on gelatin and polyvinyl alcohol-experimental studies supported by computational analysis. *Int J Mol Sci*, 22: 9909.

https://doi.org/10.3390/ijms22189909

73. Erdag D, Koc SN, Oksuzomer MF, *et al*., 2021, Synergistic effect of selenium and genipin triggers viability of 3T3 cells on PVA/gelatin scaffolds. *Acta Bioeng Biomech*, 24: 179–190.

https://doi.org/10.37190/ABB-01944-2021-04

74. Barba BJ, Oyama TG, Taguchi M, 2021, Simple fabrication of gelatin-polyvinyl alcohol bilayer hydrogel with wound dressing and nonadhesive duality. *Polym Adv Technol*, 32: 4406–4414.

https://doi.org/10.1002/pat.5442

75. George B, Bhatia N, Kumar A, *et al*., 2022, Bioinspired gelatin based sticky hydrogel for diverse surfaces in burn wound care. *Sci Rep*, 12: 13735.

https://doi.org/10.1038/s41598-022-17054-w

76. Kakarla AB, Kong I, Turek I, *et al*., 2022, Printable gelatin, alginate and boron nitride nanotubes hydrogel-based ink for 3D bioprinting and tissue engineering applications. *Mater Des*, 213: 110362.

https://doi.org/10.1016/j.matdes.2021.110362

77. Crosby CO, Stern B, Kalkunte N, *et al*., 2022, Interpenetrating polymer network hydrogels as bioactive scaffolds for tissue engineering. *Rev Chem Eng*, 38: 347–361.

https://doi.org/10.1515/revce-2020-0039